Additional plots

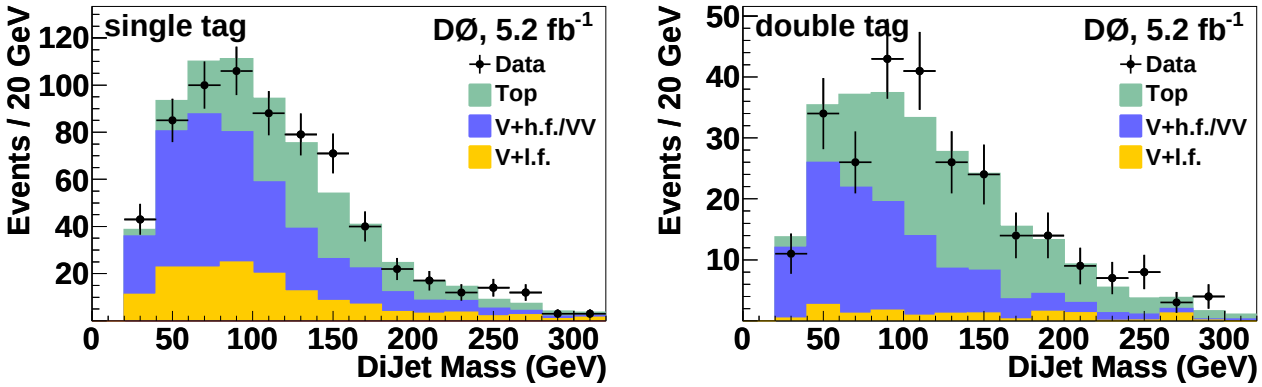

(a) (b)

FIG. 1: Dijet mass dstributions in the EW-control sample: (a) with single tag, (b) with double tag.

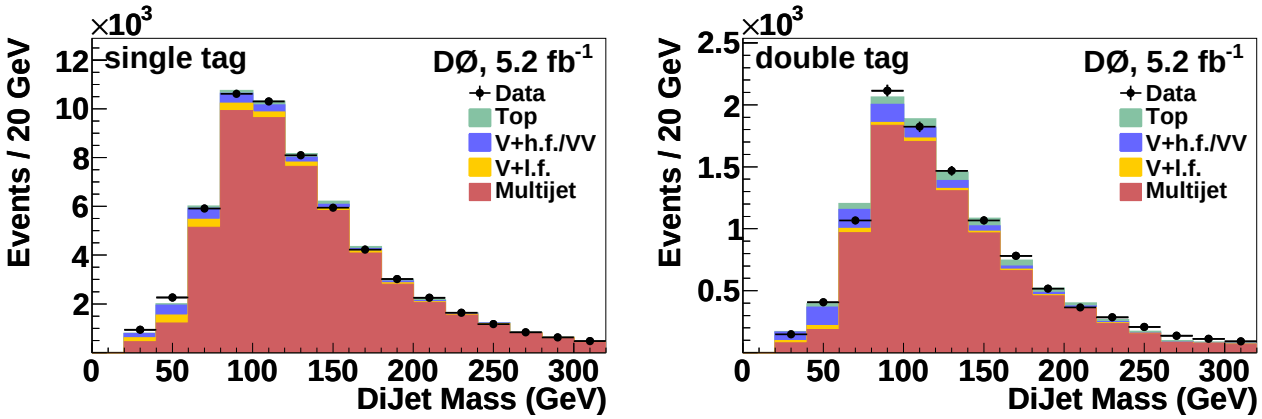

(a) (b)

FIG. 2: Dijet mass dstributions in the MJ-control sample: (a) with single tag, (b) with double tag.

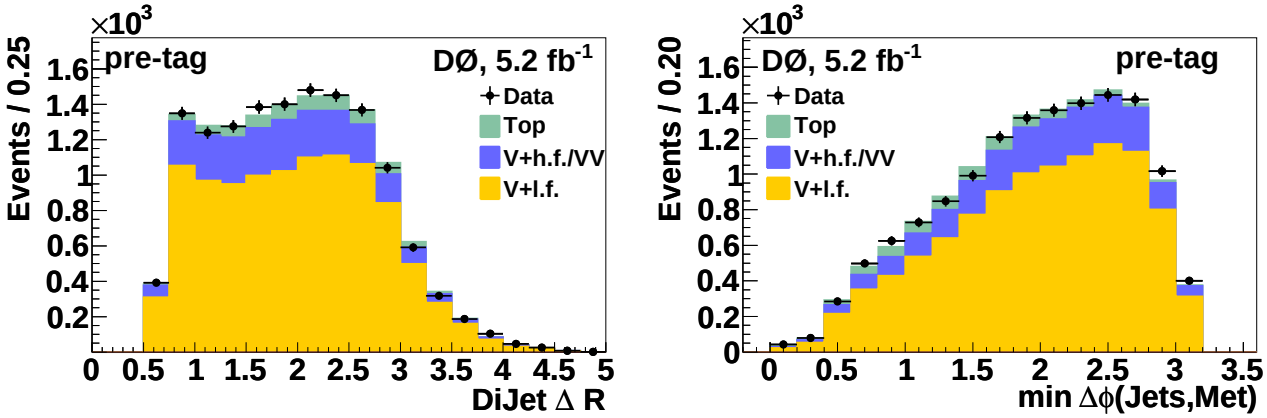

(a) (b)

FIG. 3: Distributions in the pre-tag EW-control sample: (a) Dijet ΔR, (b) Minimum $\Delta\phi$ between any jet and $\not\!\!E_T$.

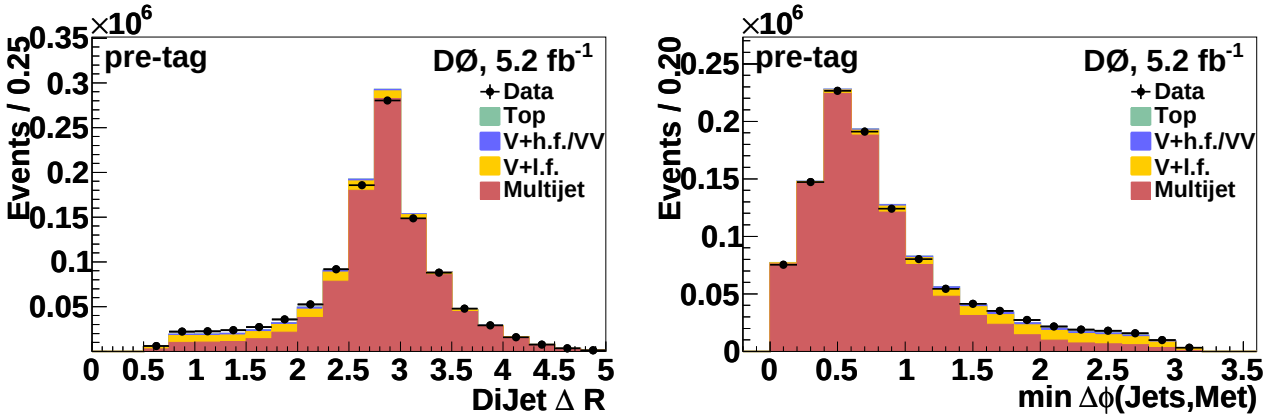

(a) (b)

FIG. 4: Distributions in the pre-tag MJ-control sample: (a) Dijet ΔR, (b) Minimum $\Delta\phi$ between any jet and $\not\!\!E_T$.

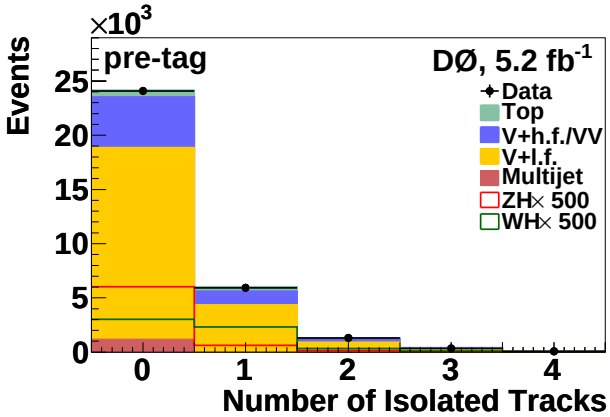

FIG. 5: Distribution of the number of isolated tracks in the analysis sample after the multijet veto. The signals are drawn separately for ZH and WH production with $m_H = 115$ GeV.

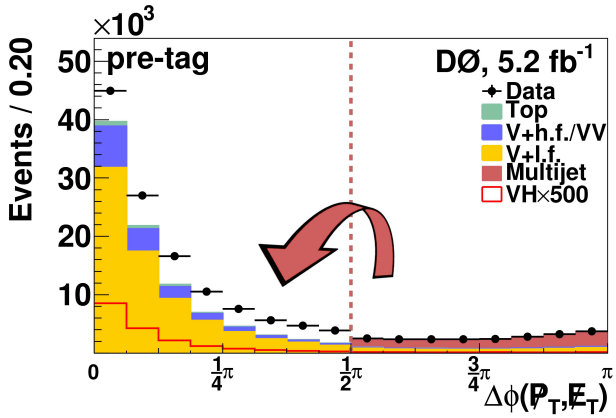

FIG. 6: Distribution of $\Delta\phi(\not{p}_T, \not{E}_T)$ in the analysis sample before the multijet veto and prior to b tagging. The data are shown as black points and the SM background prediction as stacked histograms with color codes indicated in the legend. The data events with $\Delta\phi(\not{p}_T, \not{E}_T) > \pi/2$ are used, after subtraction of the SM background contribution, to model the MJ background in the search region, i.e., for $\Delta\phi(\not{p}_T, \not{E}_T) < \pi/2$. The result, shown in brown, is further normalized to the difference between data and SM background expectation in the search region.

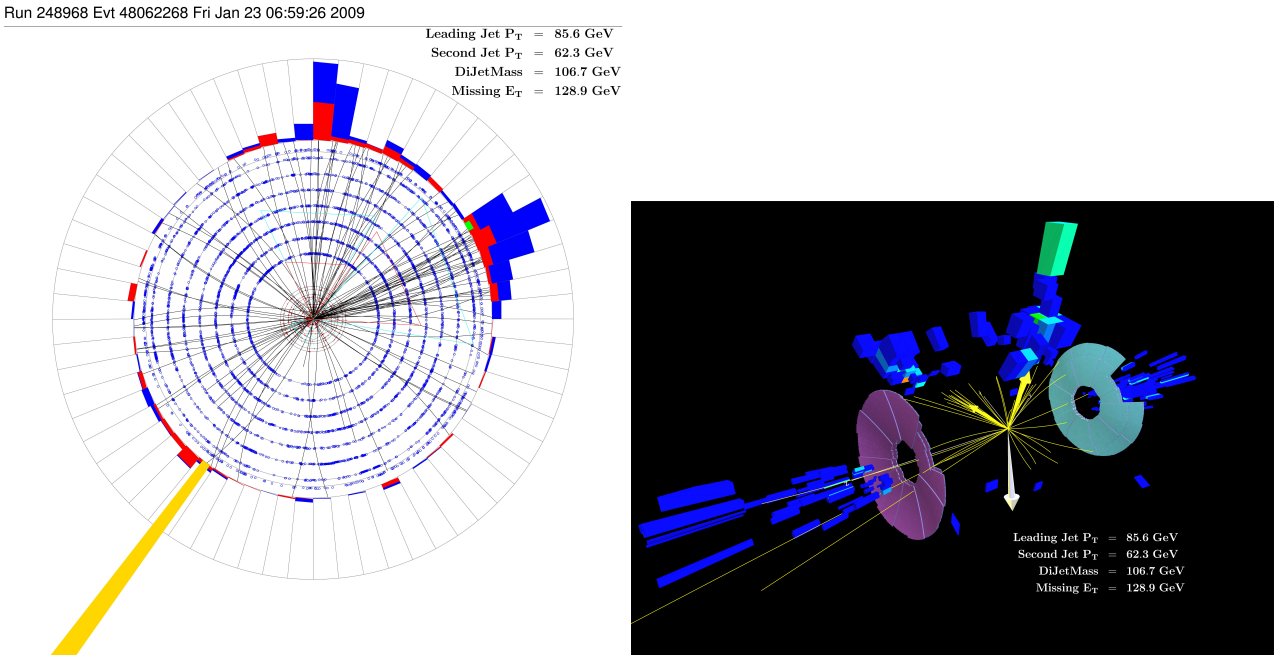

(a) (b)

FIG. 7: Displays of the most signal-like event in the double tag sample: (a) XY view, (b) 3D view. In the XY view, the transverse energy in the electromagnetic (hadronic) calorimeter is shown in red (blue), and the $\not{E}_T$ is shown in yellow. In the 3D view, the $\not{E}_T$ is shown as a white arrow, and the jets as yellow arrows, with arrow length proportional to transverse energy; the color used for the calorimeter cells becomes "warmer" as the transverse energy becomes larger; the colored disks represent the forward preshower detectors, displayed to provide orientation.